

Can we infer the percolation status of 3D fractured media from 2D outcrops?

Weiwei Zhu^a, Gang Lei^b, Xupeng He^c, Yafan Yang^d, Ryan Kurniawan Santoso^{c,e}, Moran Wang^{a,*}

^a Department of Engineering Mechanics, Tsinghua University, Beijing, China

^b Faculty of Engineering, China University of Geosciences, Wuhan, China

^c Ali I. Al-Naimi Petroleum Engineering Research Center (ANPERC), King Abdullah University of Science and Technology, Thuwal, Saudi Arabia

^d State Key Laboratory for Geomechanics and Deep Underground Engineering, China University of Mining and Technology, Xuzhou, China

^e RWTH Aachen University, Aachen, Germany

ARTICLE INFO

Keywords:

Fracture
Percolation
Multi-dimensional analysis
Connectivity
Discrete fracture network

ABSTRACT

Fractures and their connectivity are essential for fluid flow in low permeability formations. Geological outcrops can only provide two-dimensional (2D) information, but subsurface fractures are three-dimensional (3D). The percolation status of 3D fracture networks and their 2D cross-section maps are rarely investigated simultaneously. In this work, we construct 3D fracture networks with their geometries characterized by different stochastic distributions. Cross-section maps are taken to mimic real outcrops, and clusters are labeled to check the percolation status of 3D fracture networks and their 2D cross-section maps. The properties, reflecting the connectivity of two essential phases, are summarized and analyzed. We find that clustering effects impact local intersections significantly but have negligible impacts on fracture intensities of 3D fracture networks. The number of intersections per fracture is not a proper percolation parameter for complex 2D and 3D fracture networks. Real fracture networks in the subsurface should be geometrically well-connected and over-percolative if their outcrop maps have a spanning cluster formed. Empirical limits are provided to predict the fracture intensity and connectivity of subsurface 3D fracture networks based on their outcrop maps. If a spanning cluster is formed in the outcrop map, the corresponding 3D fracture networks should be over-percolative, and its fracture intensity can be larger than 3.5 times the intensity at percolation. However, if no spanning cluster is formed in the outcrop map, but the fracture intensity is larger than 0.43 times the intensity at percolation, the corresponding 3D fracture networks can form a spanning cluster and show good connectivity.

1. Introduction

Fractures play an essential role for any fluid flow in subsurface formations with low permeability, because fractures usually have much higher permeability than the matrix and serve as a high-permeable pathway to any fluid flow. Fractures are typically connected and form complex fracture networks. The connectivity of such a fracture network is crucial in flow characterizations (Berkowitz, 2002).

However, little is known about configurations of real fracture networks in the subsurface. Commonly available approaches, such as borehole images or outcrop observations (Williams and Johnson, 2004; Xu et al., 2020; Wang et al., 2021), can only provide one-dimensional or two-dimensional information. While real fracture networks in the

subsurface are always three-dimensional. 3D seismic techniques (Rijks, 1990) are available for large faults, but for fractures with a size of meters or tens of meters, they are sub-seismic patterns and can not be observed by seismic data. There are also several crosswell imaging techniques, which can resolve higher resolutions of subsurface structures, such as crosswell seismic tomography (Ellefsen et al., 2002) and crosswell electromagnetic tomography (Wilt et al., 1995). However, the well spacing limits the range of available information. Therefore, it is almost impossible to have a detailed mapping of subsurface fracture networks and evaluate their connectivity in 3D with current technologies.

Properties of 3D fracture networks in the subsurface cannot be measured directly in detail. For example, fracture intensity, P_{ij} , an essential parameter for connectivity of fracture networks, has been

* Corresponding author.

E-mail address: mrwang@tsinghua.edu.cn (M. Wang).

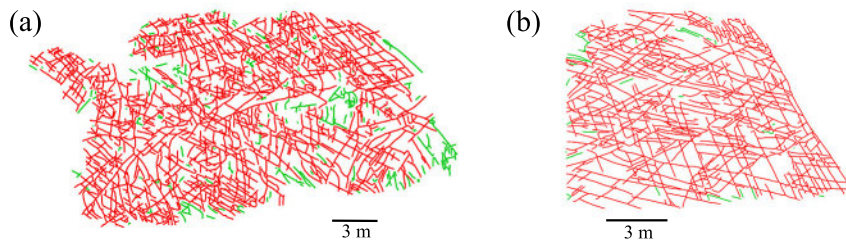


Fig. 1. Fracture outcrop map at Achnashellach Culmination field area (Fig. 7B and D in Watkins et al. (2015)). Red line segments are the largest spanning cluster; Green line segments are local clusters. (For interpretation of the references to colour in this figure legend, the reader is referred to the web version of this article.)

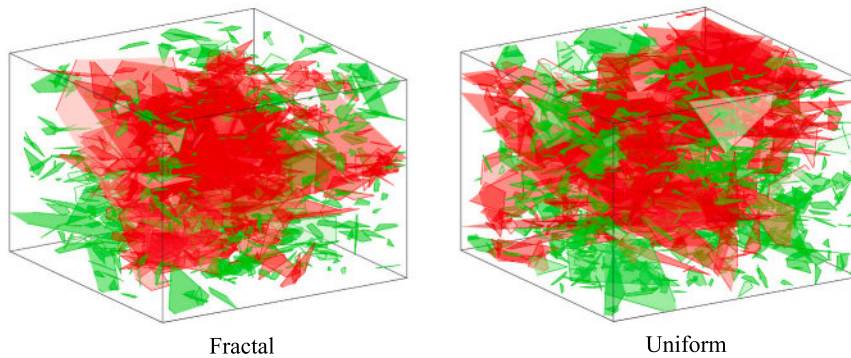


Fig. 2. 3D fracture networks. The red fractures form the connected spanning cluster. The green fractures correspond to all other locally connected clusters. In both networks, fracture orientations follow a uniform distribution, lengths obey a power-law distribution, and fracture apertures are constant. The left network has fracture center positions that follow a fractal spatial density distribution with the fractal dimension of 2.5, and in the right network, the fracture centers follow a uniform distribution. (For interpretation of the references to colour in this figure legend, the reader is referred to the web version of this article.)

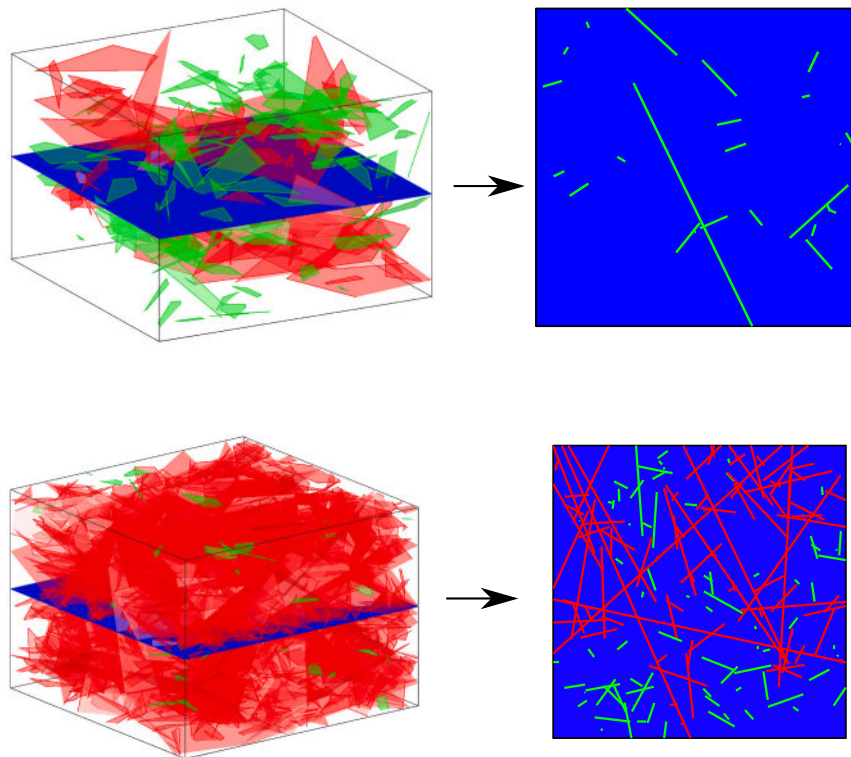


Fig. 3. A 3D fracture network and its cross-section map at the middle position. The 3D fracture network has fracture lengths following a power-law distribution with $a = 3$, positions of fracture centers following a uniform distribution, and orientations following a uniform distribution. In the 3D fracture network, red fractures form a spanning cluster that connects six faces of the domain. Green fractures are local clusters. In the 2D cross-section map, no spanning cluster is formed, and green fractures are local clusters. (For interpretation of the references to colour in this figure legend, the reader is referred to the web version of this article.)

Fig. 4. A 3D fracture network and its cross-section map at the middle position. The 3D fracture network has fracture lengths following a power-law distribution with $a = 3$, positions of fracture centers following a uniform distribution and orientations following a uniform distribution. In the 3D fracture network, red fractures form a spanning cluster which connects six faces of the domain. Green fractures are local clusters. In the 2D cross-section map, red fractures form the spanning cluster, which connects four sides of the 2D domain; green fractures are local clusters. (For interpretation of the references to colour in this figure legend, the reader is referred to the web version of this article.)

investigated extensively by correlating 3D intensities with lower-dimensional intensities mostly through stereological interpretations (Dershowitz et al., 2000). Here, P_{ij} notation conforms to the definition of Dershowitz et al. (1992), where i refers to the dimension of the sample, and j refers to the dimension of the measure. For example, P_{21} is the length of fracture traces per unit area, and P_{32} is the area of fractures per unit volume. The 1D intensity measure P_{10} and the 2D measure P_{21} are

often linearly correlated with the 3D intensity measure P_{32} under strong assumptions about the distributions of fracture lengths, positions, and orientations. However, Zhu et al. (2019) investigated the fracture intensities in different dimensions. They found that the correlation between 1D and 3D intensity parameters is weak. 2D fracture intensity parameters, such as P_{21} , have good correlations with 3D intensity parameters, such as P_{32} , if samples are correctly collected, and the number

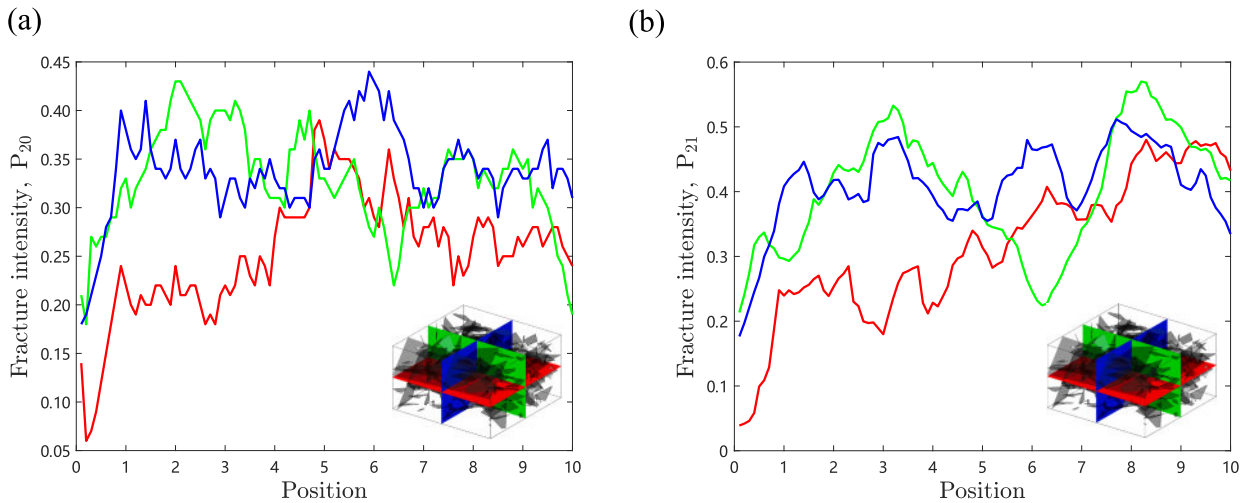


Fig. 5. Fracture intensity, P_{20} and P_{21} , of cross-section maps of a typical fracture network at different locations. The typical 3D fracture network has fracture lengths following a power-law distribution with $a = 3$, positions of fracture centers following a uniform distribution, and orientations following a uniform distribution. Cross-section maps taken from different orientations are shown in different colors.

Table 1
Summary of parameters used in the analysis.

Parameter	Definition	Usage
a	The exponent in a power-law distribution	Describing fracture lengths
F_D	The fractal dimension in a fractal spatial density distribution	Describing fracture center positions
κ	The concentration parameter in a von Mises–Fisher distribution	Describing fracture orientations
L	The system size of the fracture network	Describing system sizes
P_{20}	The number of fractures per unit area	Describing 2D fracture intensity
P_{21}	The length of fracture traces per unit area	Describing 2D fracture intensity
I_{2D}	The number of intersections per fracture in a 2D fracture network	Describing connectivity of a 2D fracture network
P_{30}	The number of fractures per unit volume	Describing 3D fracture intensity
P_{32}	The area of fracture planes per unit volume	Describing 3D fracture intensity
I_{3D}	The number of intersections per fracture in a 3D fracture network	Describing connectivity of a 3D fracture network
Number ratio (2D)	The ratio between the total number of 2D fractures at phase one and the number of 2D fractures at phase two	Linkage between Phase 1 and Phase 2
Length ratio (2D)	The ratio between the total length of 2D fractures at phase one and the length of 2D fractures at phase two	Linkage between Phase 1 and Phase 2
Number ratio (3D)	The ratio between the total number of 3D fractures at phase two and the number of 3D fractures at phase one	Linkage between Phase 2 and Phase 1
Area ratio (3D)	The ratio between the total area of 3D fractures at phase two and the area of 3D fractures at phase one	Linkage between Phase 2 and Phase 1

of independent samples is larger than 20. However, these conditions are almost inaccessible in reality. Furthermore, fracture intensity is an essential factor that impacts connectivity but cannot completely characterize it. The fracture orientations, clustering effects, and length distributions are also crucial for the system connectivity (Zhu et al., 2021c).

Percolation theory (Stauffer and Aharony, 1994) is used to study the connectivity of anything in general. The theory describes the percolation threshold, when a spanning cluster is formed in an infinitely large system, and scaling properties close to the percolation threshold. A spanning cluster refers to a large cluster connecting boundaries of the system. In particular, the connectivity of fracture networks is also heavily investigated with percolation theory considering finite-size effects (Bour

and Davy, 1997; Berkowitz et al., 2000; Masihi et al., 2007). However, the percolation status of 2D and 3D fracture networks are usually investigated as separated issues (Bour and Davy, 1997; Mourzenko et al., 2005) mostly with discrete fracture networks (DFNs). The relationship between the percolation status of 2D and 3D fracture networks is rarely investigated. In this research, the percolation status particularly refers to the formation of a spanning cluster, representing good global connectivity. The exact percolation parameter and threshold discussed in classic percolation theory are not included because the proper percolation parameter for complex fracture networks is still unclear. From our previous research (Zhu et al., 2018), we found that commonly used quantities (total excluded area, total self-determined area, and the number of intersections per fracture) are not appropriate percolation parameters for complex fracture networks, where fracture lengths follow a power-law distribution and positions of fracture centers follow a fractal spatial density distribution. Therefore, finding a proper percolation parameter and its threshold is still an open issue, which should depend on specific configurations of fracture networks and be valid in an infinitely large system. In this work, three states are considered for fracture networks to describe different degrees of percolation, which are percolative, under-percolative, and over-percolative states. The percolative state is the critical point when the spanning cluster is formed. The under-percolative state refers to sparse fractures, and only local clusters are formed. The over-percolative state is when a spanning cluster is formed, and the fracture intensity is much higher than the intensity at the percolative state.

Outcrop maps provide abundant resources to observe natural fractures exposed on the surface. If the rock types and structural settings of the surface outcrops and subsurface formations are similar, outcrop analogs can be regarded as relevant to the subsurface formation. From a collection of 80 outcrops in our previous research (Zhu et al., 2021a), we find that most natural outcrop maps show good geometrical connectivity, and 63 out of 80 outcrop maps have formed a spanning cluster that connects the outcrop map’s boundaries. For small-scale (<100 m) outcrop maps, such proportion is much higher. One example of outcrop maps at Achnashellach Culmination field area (Watkins et al., 2015) is shown in Fig. 1, where the largest cluster is marked in red, and the other small clusters are marked in green. Outcrops are processed with an automatic fracture detection algorithm (Zhu et al., 2021a), where raw outcrops are converted to polylines for calculations.

However, an outcrop map can only be considered as a cross-section map of the actual 3D fracture network. From well-connected 2D outcrop maps, can we infer good connectivity of corresponding 3D

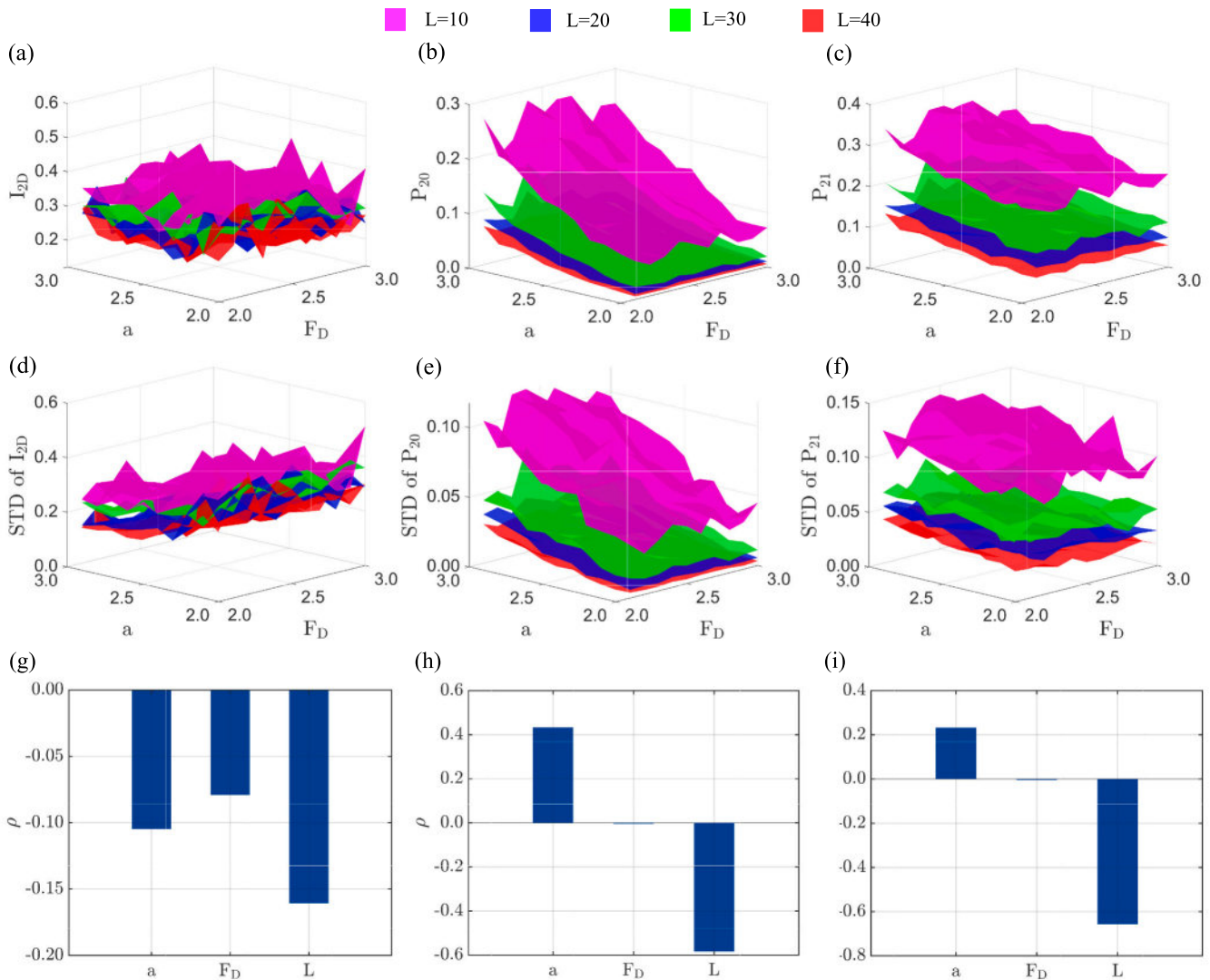


Fig. 6. Results of 2D cross-section maps at phase one, where a spanning cluster is formed in each 3D fracture network. (a-c) show I_{2D} , P_{20} and P_{21} of 2D cross-section maps averaged over 50 realizations. (d-f) show standard deviations of each parameter in the first row. (g-i) show the sensitivity rank of each geometrical parameter (a , F_D , L) with each parameter in the first row as the response.

fracture networks? Do 3D fracture networks also form the spanning cluster? Can 3D fractures be over-percolative? This information is essential to evaluate the geometrical connectivity of fracture networks in the subsurface but is rarely investigated. This work focuses on the geometrical connectivity instead of the conductivity of fracture networks. The latter involves significant complexities, including complex fracture shapes, fracture roughness, the tortuosity of the flow paths in fractures, the stress and diagenesis impact, which change the fracture aperture significantly. Incorporating those complexities in complicated fracture networks is computationally unacceptable. However, the geometrical connectivity is a premise for fluid flow in low permeability formations, because fluid flow happens in connected instead of isolated fractures, and flow results, such as flow rate or flow-based permeability, are sensitive to fracture network configurations. Therefore, this work aims to explore the percolation status of 2D cross-section maps and their corresponding 3D fracture networks.

In this research, we adopt the DFN (discrete fracture network) method (Lei et al., 2017) and generate 3D fracture networks with their geometries, such as fracture sizes, orientations, and positions of fracture centers, following different stochastic distributions. We also change the system size and evaluate finite-size effects. Cross-section maps are taken to mimic real outcrops. Then, clusters are labeled to check the

percolation status of the 3D fracture network and their 2D cross-section maps. The properties, reflecting the connectivity of two important phases, are summarized and analyzed. The properties include P_{30} , P_{32} and I_{3D} for 3D fracture networks, and P_{20} , P_{21} and I_{2D} for 2D cross-section maps. I_{3D} and I_{2D} are the number of intersections per fracture for a 3D fracture network and 2D cross-section map, respectively. Although none of those parameters can completely characterize the connectivity of a fracture network, they are convenient to quantify and usually adopted as the termination criterion in DFN modelings, especially for fracture intensities. Two critical phases are considered, including i, when the spanning cluster is formed in the 3D fracture network, indicating good connectivity of the 3D fracture network; ii, when a spanning cluster is formed in the 2D cross-section map, indicating good connectivity in 2D cross-section maps. The simulation in this research is conducted with in-house software, HatchFrac, efficient software to generate discrete fracture networks in 2D and 3D (Zhu et al., 2021b).

The remainder of this paper is organized as follows: In Section 2, techniques to construct a 3D fracture network and take cross-section maps are introduced. Impacts of fracture geometries (lengths and center positions) and system sizes on the connectivity are studied with the sensitivity analysis method, which is also introduced in Section 2. In

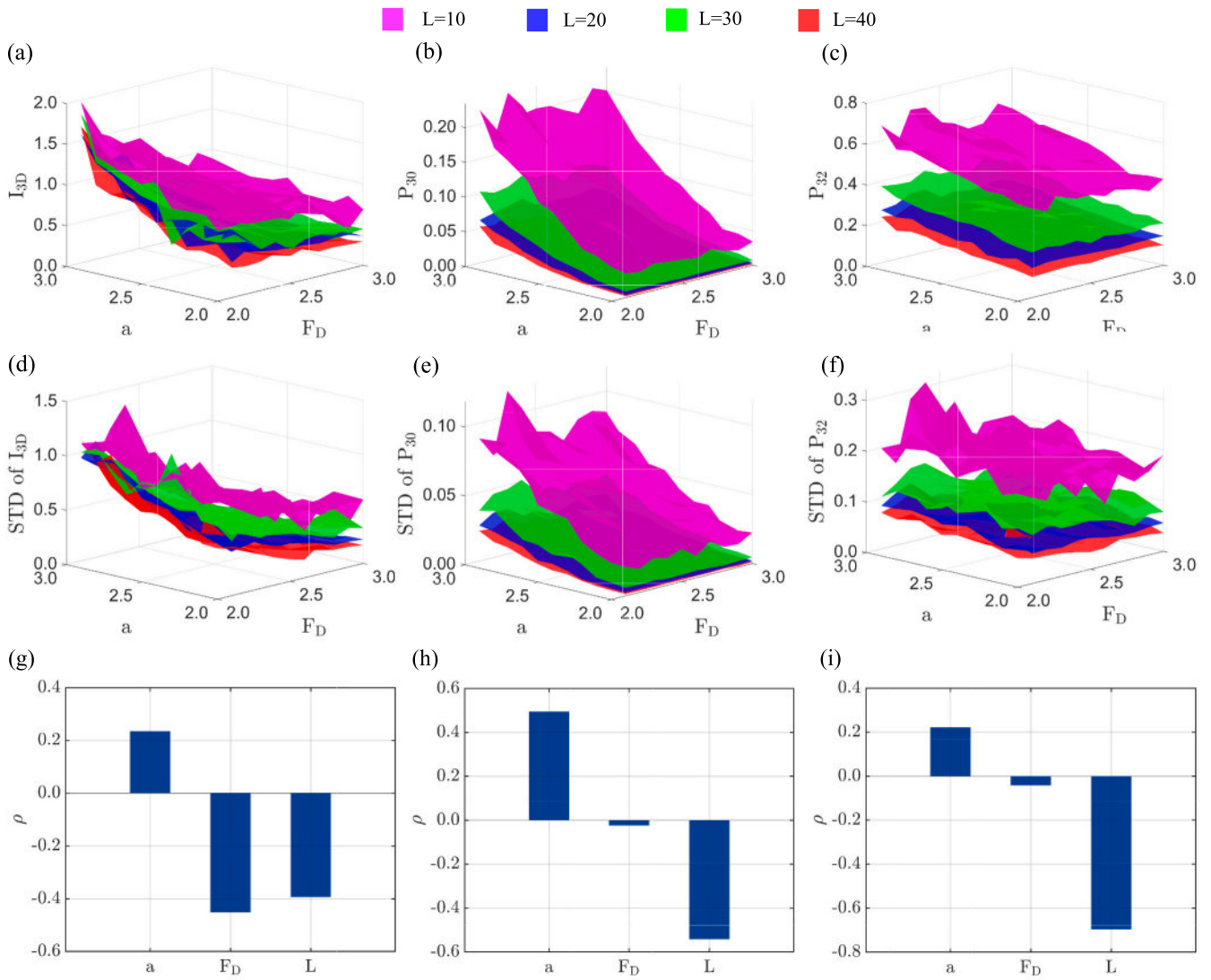


Fig. 7. Results of 3D fracture networks at phase one, where a spanning cluster is formed in each 3D fracture network. (a-c) show I_{3D} , P_{30} and P_{32} of 3D fracture networks averaged over 50 realizations. (d-f) show standard deviations of each parameter in the first row. (g-i) show the sensitivity rank of each geometrical parameter (a , F_D , L) with each parameter in the first row as the response. In subfigure (a), I_{3D} has been corrected for the finite-size effect.

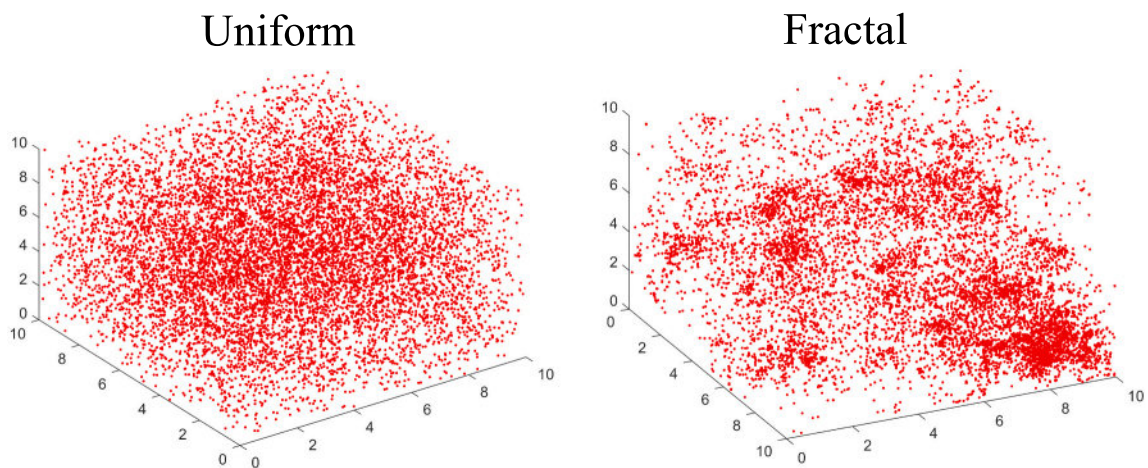


Fig. 8. 10,000 3D spatial points follow a uniform (Left) or a fractal spatial density distribution (Right) with the fractal dimension $F_D = 2.1$.

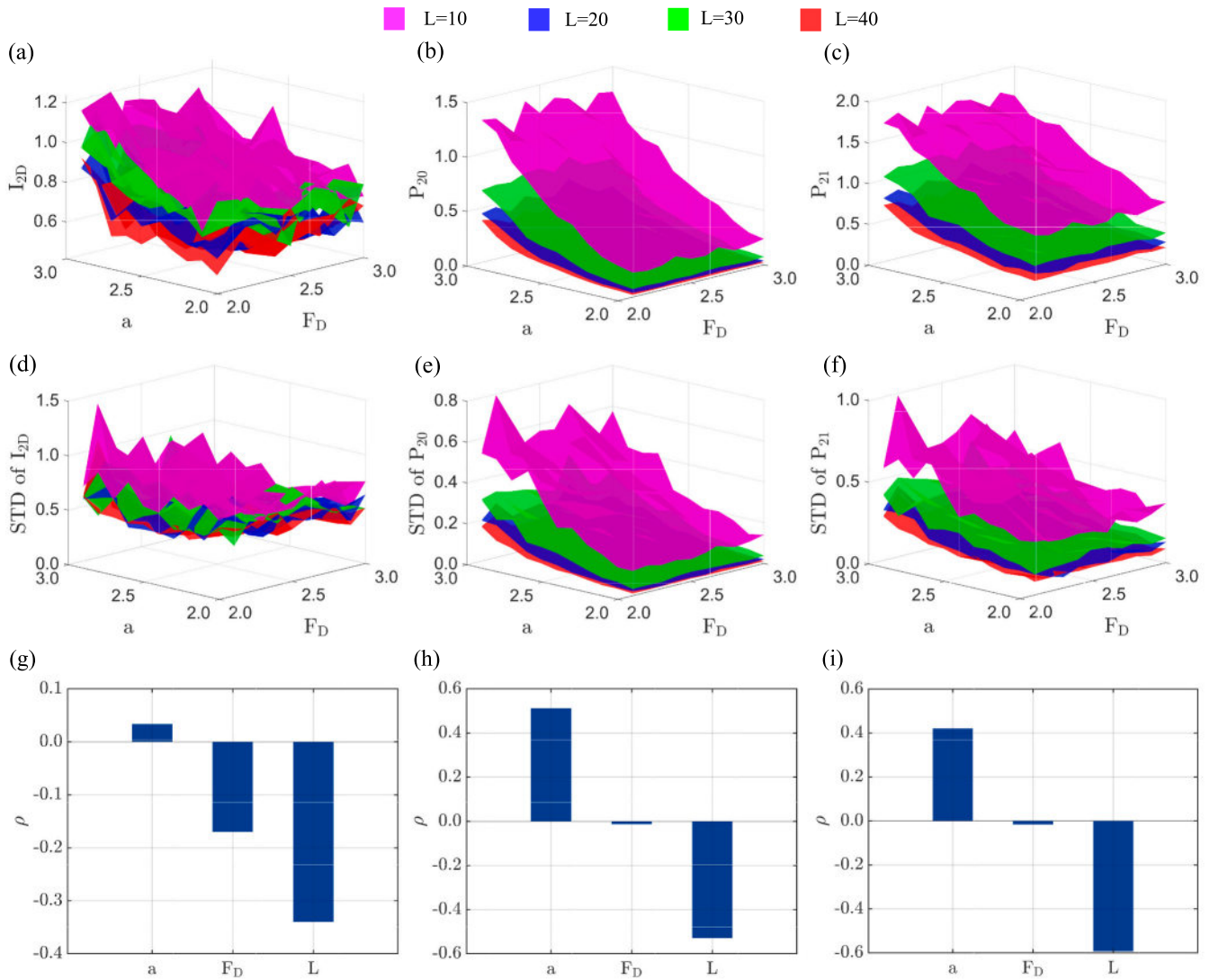


Fig. 9. Results of 2D cross-section maps at phase two, where a spanning cluster is formed in the cross-section map. (a-c) show I_{2D} , P_{20} and P_{21} of 2D cross-section maps averaged over 50 realizations. (d-f) show standard deviations of each parameter in the first row. (g-i) show the sensitivity rank of each geometrical parameter (a , F_D , L) with each parameter in the first row as the response. In subfigure (a), I_{2D} has been corrected for the finite-size effect.

Section. 3, results on the percolation status of 3D fracture networks and their cross-section maps are presented. The properties at two critical phases are analyzed in detail. In Section. 4, we discuss the percolation status in realistic fracture networks and real outcrops. Important conclusions are summarized in Section. 5.

2. Materials and methods

This section introduces procedures to generate 3D fracture networks, take 2D cross-section samples and check clusters in both 2D and 3D fracture networks.

2.1. Generation of 3D fracture networks and cluster-check

Subsurface fracture networks are complex, and it is almost impossible to map them accurately. The DFN modeling is a practical alternative to represent complex fracture networks with simplified geometries. In this research, random convex polygons with four vertices are adopted to represent fractures in 3D. The random polygon reserves certain degrees of irregularity compared with a disk or ellipse shape. It is also straightforward to convert convex polygons to elliptical shapes or other

polygonal shapes by adding a few more vertices and minor adjustments to the coordinates. Furthermore, the intersection analysis of convex polygons is much more convenient than that of ellipses. Jing and Stephansson (2007) figured out that the significance of fracture shapes decreases with an increase in the fracture population size.

Three key geometrical parameters are adopted to describe a fracture network, including fracture lengths (sizes), orientations, and positions of fracture centers. Different stochastic distributions are summarized mainly from outcrop or experiment observations to characterize those geometrical parameters (Zhu et al., 2021a).

A power-law distribution (Bour and Davy, 1997) is dominantly used to describe fracture length, probably due to the self-similarity of natural fractures (Makarov, 2007).

$$n(l) = al^{-a}, \tag{1}$$

where $n(l)dl$ is the number of fractures with lengths ranging from $[l, l + dl]$, a is the proportionality coefficient and a is the power-law exponent. The power-law exponent has to be larger than one, and usually ranges between 2.0 and 3.0 for most cases (Bonnet et al., 2001; Zhu et al., 2018). The exponent controls the probability of generating long fractures, and the probability of generating very long fractures decreases

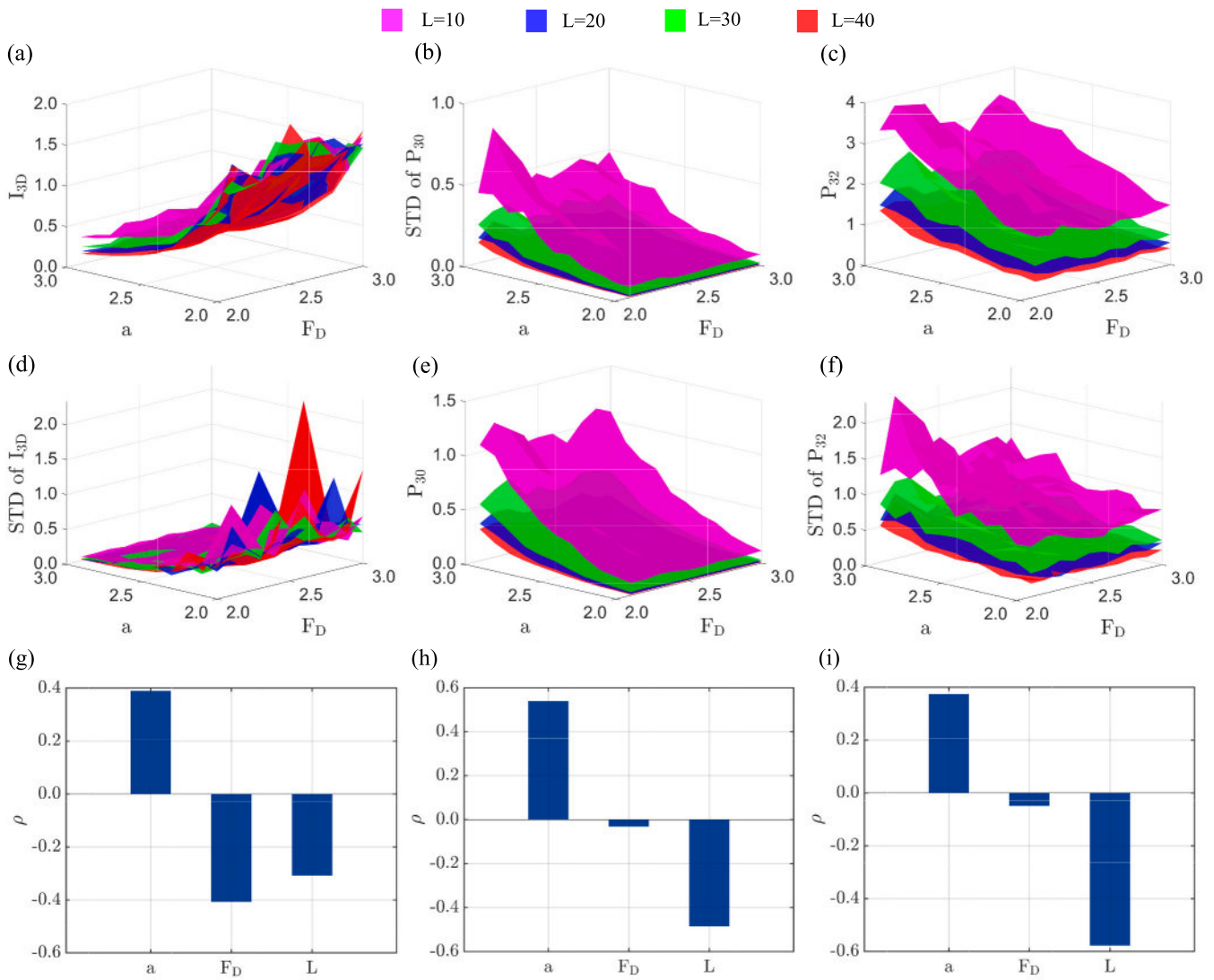


Fig. 10. Results of 3D fracture networks at phase two, where a spanning cluster is formed in the cross-section map. (a-c) show I_{3D} , P_{30} and P_{32} of 3D fracture networks averaged over 50 realizations. (d-f) show standard deviations of each parameter in the first row. (g-i) show the sensitivity rank of each geometrical parameter (a , F_D , L) with each parameter in the first row as the response.

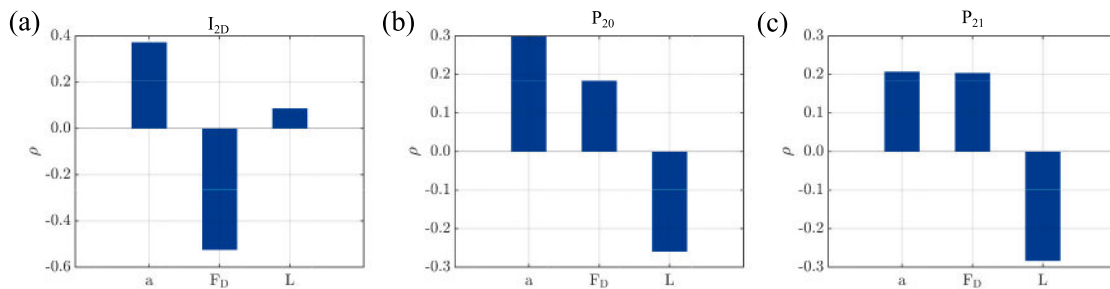


Fig. 11. Sensitivity ranks of the exponent (a), fractal dimension (F_D) and system sizes L on the I_{2D} , P_{20} and P_{21} in 2D fracture networks.

sharply as a increases. 3D fractures are represented with planar polygons. Therefore fracture lengths are inappropriate to describe their sizes. Firstly, convex polygons are generated with the side length randomly varying between 0 and 1; A scaling operation is then performed on the polygon with a scale factor of l to change their sizes.

The fracture orientations are highly stress-dependent, depending on the current stress field and the history of stress changes. Over the long geologic history, subsurface rocks may have many different sets of

fractures because of stress variations (Barton and Larsen, 1985). A von Mises–Fisher distribution (Whitaker and Engelder, 2005) is commonly adopted to describe fracture orientations. From outcrop observations, the concentration parameter κ in the distribution is usually small and makes the distribution close to a uniform distribution (Zhu et al., 2021a). Therefore, fracture orientations follow a uniform distribution between 0 and π for strikes and dips in this research.

The positions of fracture centers are described by a uniform or fractal

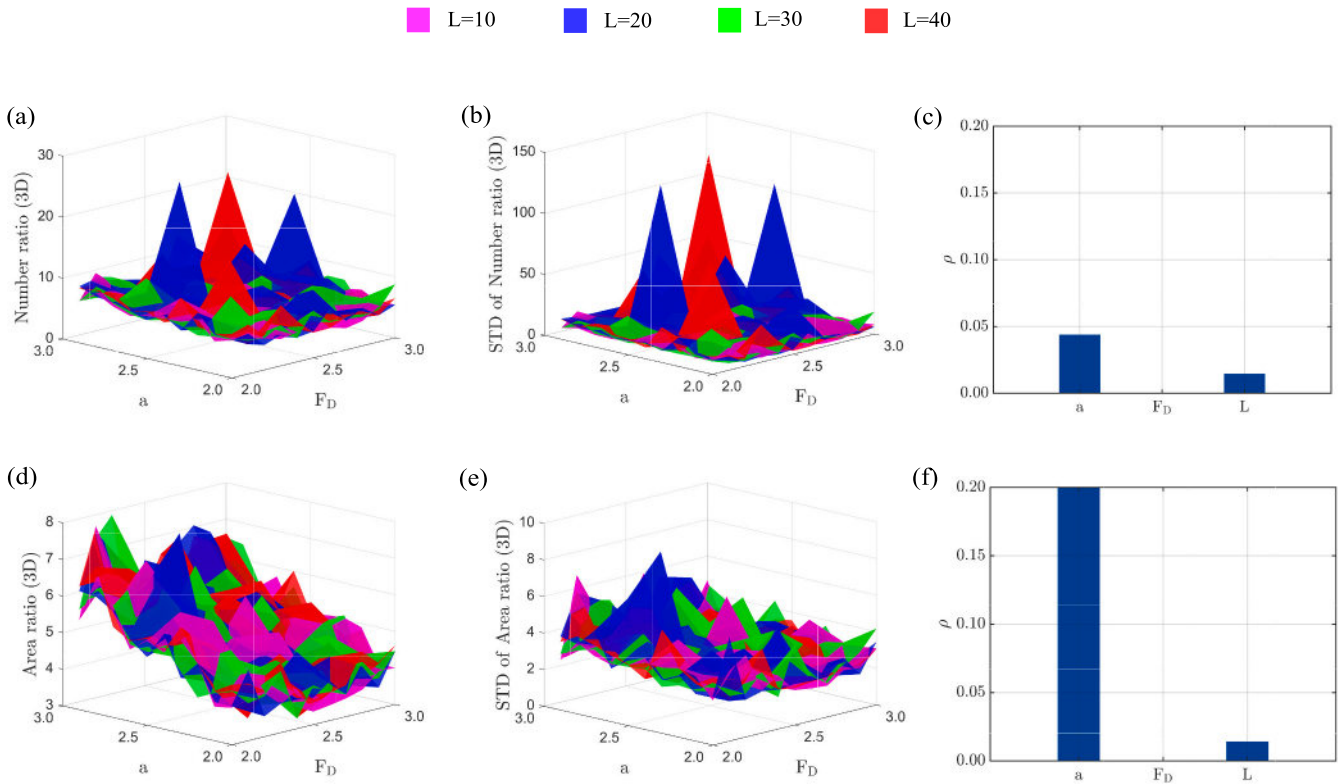


Fig. 12. (a,d) mean values of the number ratio and area ratio; (b,e) standard deviations of the number ratio and area ratio; (c,f) sensitivity ranks of geometrical parameters (a , F_D , L) with the number ratio and area ratio as the response. The number ratio/ area ratio refer to ratios between the total number/area of 3D fractures at phase two and the total number/area of 3D fractures at phase one.

spatial density distribution (Bour and Davy, 1997; Zhu et al., 2018). The former one is simple for implementation but not realistic since many outcrop maps show clustered natural fractures (Zhu et al., 2018; Akara et al., 2021). The fractal spatial density distribution introduces clustering effects, characterized by a fractal dimension, F_D . For a three-dimensional space, the fractal dimension varies between 2.0 and 3.0, while a smaller fractal dimension refers to more severe clustering effects.

After determining the stochastic distributions, we can generate each fracture and form complex networks by adding fractures in succession. Fracture terminations (T-type intersections) are not included in this work. However, the results are still reasonable because fracture terminations have limited contributions to the connectivity compared with fracture intensities, lengths, and positions. To check the percolation status of fracture networks, we need to find fracture clusters and label them. In this research, we extend a fast Monte Carlo algorithm by Newman and Ziff (2001) to check clusters instead of the commonly used Hoshen-Kopelman algorithm (Hoshen and Kopelman, 1976). The efficiency is significantly enhanced and makes it practical to check clusters for large systems and thousands of realizations. The termination of generating new fractures can be any user-defined criterion, such as a given fracture intensity or the formation of a spanning cluster.

The fracture network is generated with in-house built DFN software, HatchFrac, and detailed procedures and algorithms are available from Zhu et al. (2021b). Fig. 2 shows examples of 3D fracture networks with their geometries characterized by stochastic distributions listed above. The termination criterion is forming a spanning cluster (red cluster), which connects six faces of the 3D domain.

2.2. Cross-section of 3D fracture networks and cluster-check

Outcrop maps are spread worldwide and provide abundant resources to study natural fracture networks. However, outcrops are only 2D cross-

section maps of an entire 3D fracture network, where the ground surface serves as the cross-sectional plane. Furthermore, weathering and complex surface topography can cause outcrops to differ from the subsurface systems significantly (Ukar et al., 2019). In addition, the significant stress release experienced by subsurface rocks during the upward movement may also change the fracture network configuration. The published outcrop maps usually bias samples where outcrops with well-developed fractures are preferred. Therefore, in this work, we assume that.

- Samples of outcrop maps are unbiased and can represent natural fracture networks.
- Outcrop maps on the surface can be related to subsurface structures and are similar to the cross-section map of the subsurface fracture network.
- DFNs (discrete fracture networks) are representative of natural fracture networks.

How to link the connectivity of 2D outcrops and their corresponding 3D structures remains an open issue because the actual 3D structures are almost inaccessible with current technologies. With the 3D fracture networks generated in the previous section, we can investigate the problem reversely. By taking 2D cross-section maps from the 3D fracture network, we mimic the 2D outcrop maps and explore the percolation status and the relationship between 2D outcrops and their 3D structures.

The method to take the cross-section map is trivial.

- First, define a cross-sectional plane based on a given orientation and position.
- Second, find all the intersection lines between the cross-sectional plane and all fractures in the 3D fracture network.

The cross-section map of the 3D fracture network is a 2D fracture network. The same cluster-check algorithm can be implemented to check clusters in cross-section maps. Fig. 3 and Fig. 4 provide two

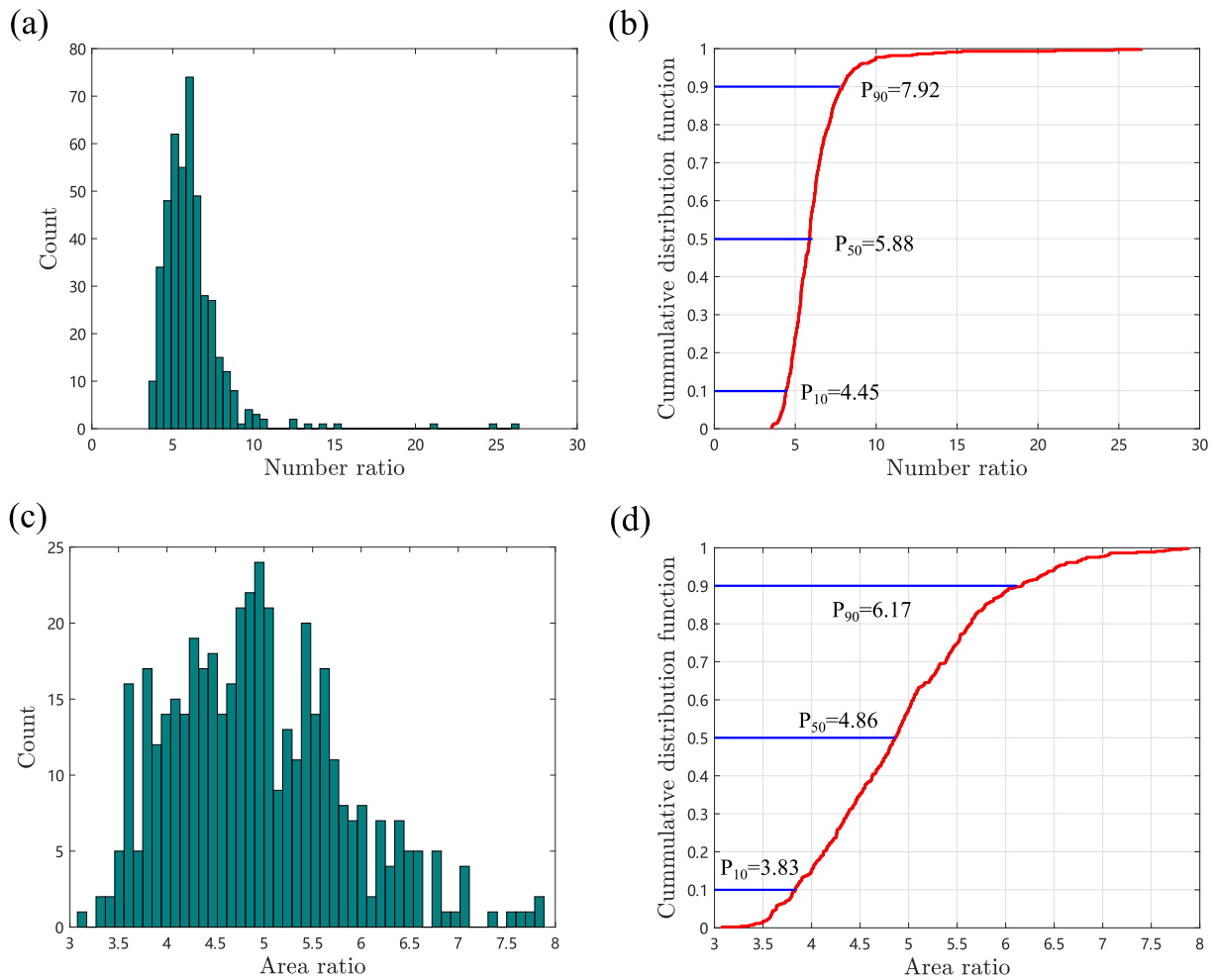


Fig. 13. (a,c) The histogram of the number ratio and area ratio; (b,d) The cumulative distribution function of the number ratio and area ratio.

Table 2
Statistics of parameters in two phases.

Parameter	Number ratio (3D)	Area ratio (3D)	Number ratio (2D)	Length ratio (2D)
Max	26.4	7.9	0.43	0.41
Min	3.5	3.1	0.16	0.17
Mean	6.1	4.9	0.29	0.28
Median	5.9	4.9	0.28	0.27
STD	2.1	0.9	0.05	0.05
P_{10}	4.5	3.8	0.22	0.21
P_{50}	5.9	4.9	0.29	0.27
P_{90}	8.2	6.2	0.37	0.35

examples of a cross-section map taken from a 3D fracture network. The percolation status of the 2D cross-section maps in the two examples are different. In Fig. 3, the 3D fracture network has formed a spanning cluster, suggesting good connectivity, but no spanning cluster is formed in the cross-section map. In Fig. 4, both 3D fracture network and its cross-section map have a spanning cluster formed. The spanning cluster for both 3D fracture networks and 2D cross-section maps are shown in red. The fracture intensity in Fig. 4 is almost three times larger than the intensity in Fig. 3. Therefore, good connectivity in 3D structures cannot ensure good connectivity in 2D outcrop maps. In reverse, good connectivity in outcrop maps may suggest an over-percolative status of the corresponding 3D fracture network.

It is worth mentioning that fracture intensities of cross-section maps vary at different positions. Fig. 5 shows fracture intensities, P_{20} and P_{21} ,

at different positions in three directions for a typical 3D fracture network. The fracture intensities near boundaries are usually small. However, the spatial variations inside the domain are uncertain, depending on the geometrical properties of fracture networks (e.g., clustering effects). It is unpractical and unnecessary to have many 2D cross-section maps with limited computational resources. Therefore, we choose the cross-section map at the middle position (blue plane) of the domain as a representative to investigate the percolation status of different dimensional fracture networks since it usually has an intermediate intensity value.

In summary, this research investigates the percolation status and connectivity of 3D fracture networks and their cross-section maps. In particular, we generate fracture networks in 3D and stop generating new fractures when the 2D cross-section map forms a spanning cluster. This process includes two critical phases. The first phase is when the spanning cluster is formed in the 3D fracture network, indicating good connectivity for the 3D fracture network. The second phase is when a spanning cluster is formed in the 2D cross-section map, indicating good connectivity for 2D cross-section maps. Several key parameters, essential for connectivity, are summarized from each realization at both phases, including P_{30} , P_{32} and I_{3D} for 3D fracture networks, and P_{20} , P_{21} and I_{2D} for 2D cross-section maps. P_{ij} refers to fracture intensity, and I_{2D} and I_{3D} focus on the intersections. Both of them are essential to evaluate the connectivity of a fracture network.

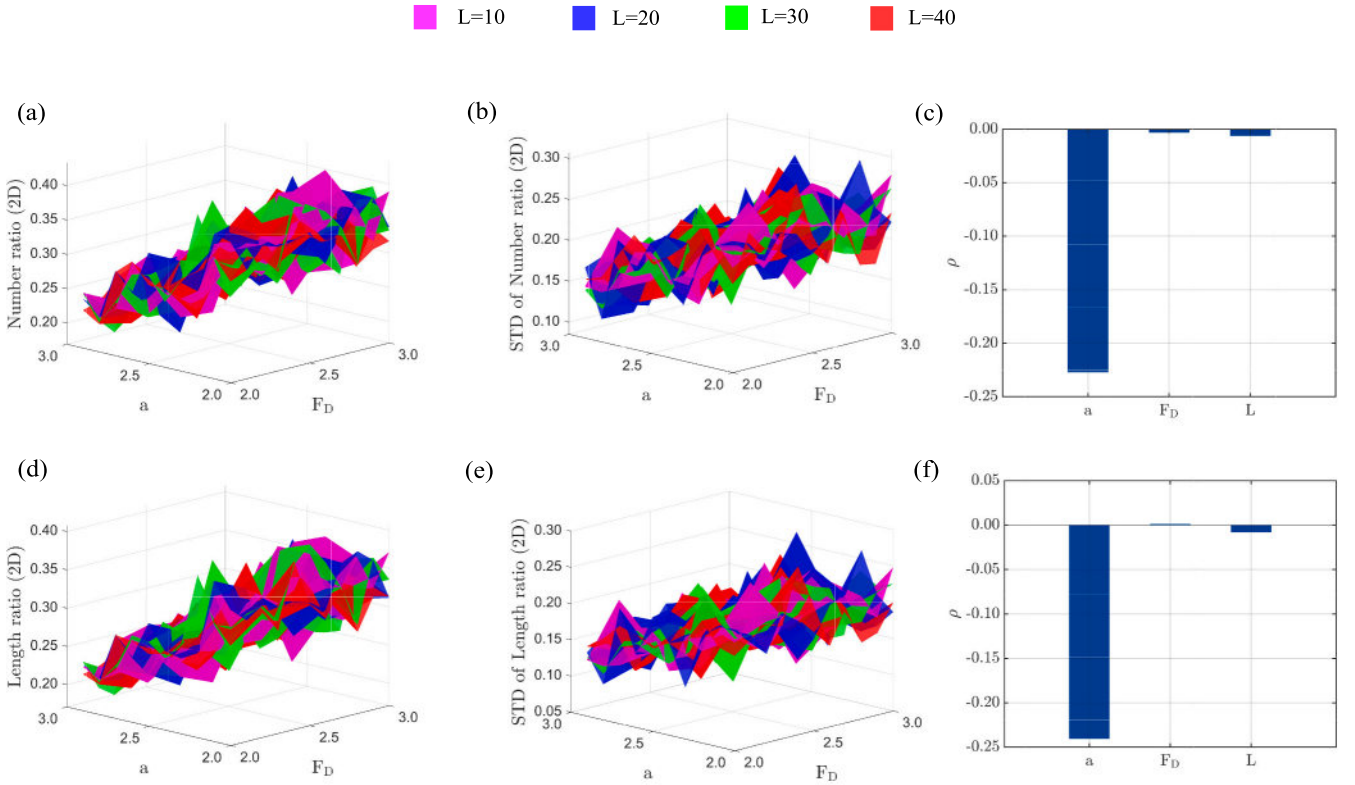


Fig. 14. (a,d) mean values of the number ratio and length ratio; (b,e) standard deviations of the number ratio and area ratio; (c,f) sensitivity ranks of geometrical parameters (a , F_D , L) with the number ratio and length ratio as the response. The number ratio/ length ratio refer to ratios between the total number/length of 2D fractures at phase one and the total number/length of 2D fractures at phase two.

2.3. Sensitivity analysis

We investigate the impacts of critical geometrical properties, including fracture lengths, positions of fracture centers, and system sizes, on the connectivity of 3D fracture networks and their 2D cross-section maps. As discussed in the previous section, different stochastic distributions are implemented to describe fracture geometries. The power-law exponent, a , usually varies between 2.0 and 3.0 (Zhu et al., 2018), and we take 11 values from 2.0 to 3.0 with a step of 0.1. The fractal dimension, F_D , for 3D fracture networks should be larger than 2.0 but smaller than 3.0. We take 10 values from 2.1 to 3.0 with a step of 0.1. The system size, L , is chosen from 10 to 40 with a step of 10. Each case is stabilized by averaging over 50 realizations.

To quantify the impact of each geometrical parameter on the connectivity, a sensitivity analysis is necessary. Different geometrical properties are assumed to be independent of each other. The input/output correlation method is applicable, in which the sensitivity of model response Y to the components of the input random vector X is calculated by determining the component-wise correlation coefficients between the two. Consider n samples of the input random vector $X = \{x^{(1)}, x^{(2)}, x^{(3)}, \dots, x^{(n)}\}$, and the corresponding model responses $Y = \{y^{(1)}, y^{(2)}, y^{(3)}, \dots, y^{(n)}\}$. The linear correlation coefficient ρ_i between the i^{th} input and output is defined as

$$\rho_i = \rho(X_i, Y) = \frac{E[(X_i - \mu_i)(Y - \mu_Y)]}{\sigma_i \sigma_Y}, \quad (2)$$

where μ_i and μ_Y are the expected values of X_i and Y respectively, and σ_i and σ_Y are the corresponding standard deviations. The importance of each factor is ranked based on the correlation coefficient. The response can be any recorded parameter mentioned above, which reflects the connectivity of the fracture network, and the input vector includes a , F_D , and L for both the 2D and 3D fracture networks.

Table 1 summarizes all parameters used in this work, including parameters of fracture geometries, parameters of fracture intensities and intersections, and parameters linking two phases.

3. Results

This section presents results of I_{2D} , P_{20} and P_{21} of 2D cross-section maps and I_{3D} , P_{30} and P_{32} of corresponding 3D fracture networks in two critical phases. The sensitivity analysis of geometrical properties, including the power-law exponent (a), fractal dimension (F_D) and system size (L), are provided.

3.1. Results in phase one

When a spanning cluster is formed in 3D fracture networks, their cross-section maps are usually poorly connected, and there is no spanning cluster formed in cross-section maps. Fig. 6(a-c) show I_{2D} , P_{20} and P_{21} of 2D cross-section maps averaged over 50 realizations. Fig. 6(d-f) show standard deviations of each parameter in the first row. Fig. 6(g-i) show the sensitivity rank of each geometrical parameter (a , F_D , L) with each parameter in the first row as the response. Similarly, Fig. 7 shows variations of I_{3D} , P_{30} and P_{32} of 3D fracture networks.

In Fig. 6(a), the number of intersections per fracture (I_{2D}) is low. For many cases, there is no intersection at all and yields zero for I_{2D} . In Fig. 6 (b, c), P_{20} and P_{21} have similar behaviors. They have low values and decrease with system sizes. The standard deviations of P_{20} and P_{21} decrease with increasing system sizes. From the sensitivity analysis, the exponent a and system size L have strong correlations with P_{20} and P_{21} . The exponent a has a strong positive correlation with these two parameters, indicating that fracture networks dominated by small fractures tend to have high fracture intensities. The system size L has a strong negative correlation with P_{20} and P_{21} , indicating that large system may have sparse fracture networks. The fractal dimension F_D ,

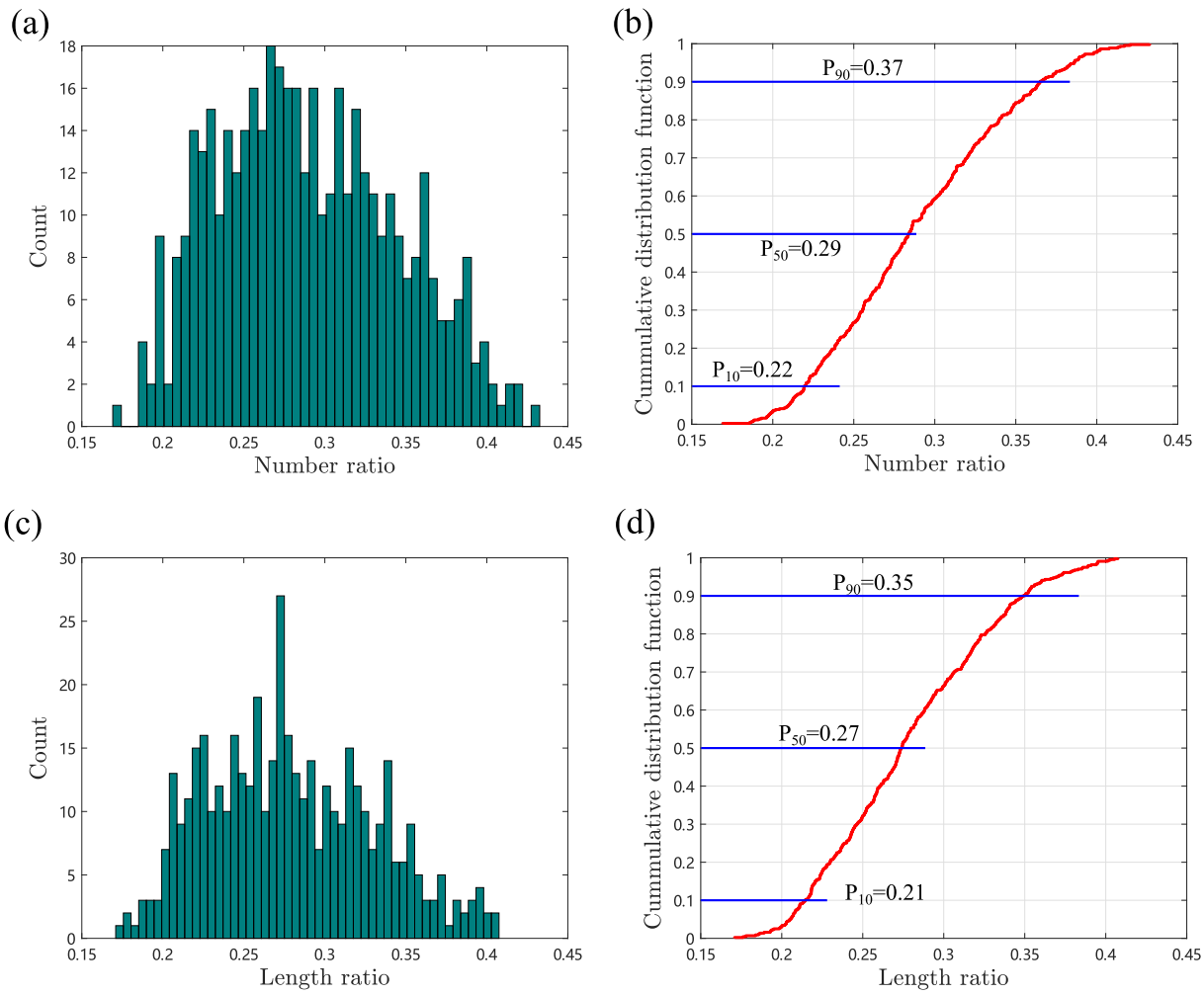


Fig. 15. (a,c) The histogram of the number ratio and length ratio; (b,d) The cumulative distribution function of the number ratio and length ratio.

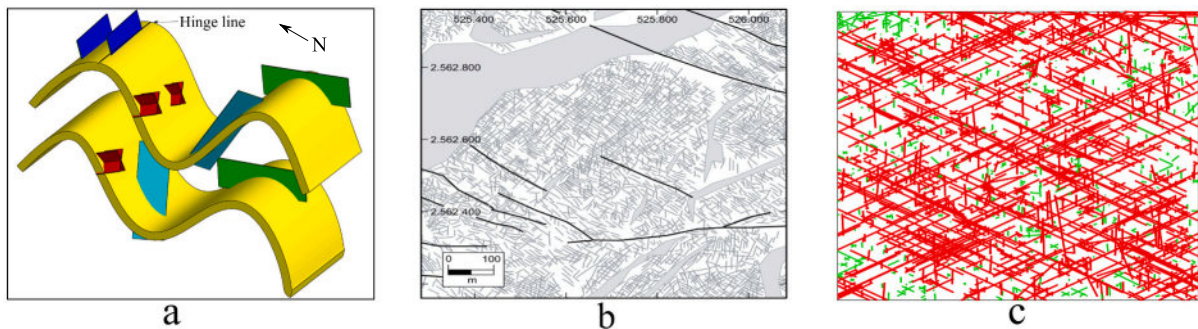


Fig. 16. (a) A sketch map to illustrate four types of joints in a fold structure; (b) An outcrop map from Holland et al. (2009a); (c) A cross-section map of our fracture network. Red fractures are the largest cluster; Green fractures are local clusters. (For interpretation of the references to colour in this figure legend, the reader is referred to the web version of this article.)

representing clustering effects, has almost no correlation with fracture intensities.

For phase one, there is a spanning cluster formed in 3D fracture networks. The number of intersections per fracture (I_{3D}) has been regarded as the percolation parameter for fracture networks (Robinson, 1983). However, Zhu et al. (2018) showed that this parameter is not a valid percolation parameter in complex 2D fracture networks. Here, we can further check the applicability of this parameter as a percolation parameter in 3D fracture networks with available data. For a quantity to

be a valid percolation parameter, this quantity has to fulfill two requirements: i, there should be finite-size effects in a system with a finite size; ii, the quantity should yield a constant percolation threshold in an infinitely large system or a finite system after correcting for finite-size effects. Percolation theory describes the global connectivity in an infinitely large system. However, the fracture network generated always has a finite size. Therefore, the finite-size effect should be accounted for (Bour and Davy, 1997)

$$p_c(L) - p_c^\infty \sim \Delta p_c(L), \tag{3}$$

Table 3
Distributions of each type of joints.

Type of joints	Probability ^a	Center position	Strike	Dip	Length
1	0.02	Uniform ^b	von Mises-Fisher ($\mu = 90^\circ, \kappa = 300$)	90°	2 L
2	0.02	Uniform	von Mises-Fisher ($\mu = 0^\circ, \kappa = 300$)	90°	Power-law ^e ($L_{max} = L, a = 3$)
3	0.72	Uniform	^d N60°E, S60°E	90°	Power-law ($L_{max} = L, a = 2.5$)
4	0.24	Fractal ^c	Uniform ([0, 2 π])	Uniform ([0, 2 π])	Power-law ($L_{max} = L, a = 3$)

^a probability of generation.

^b a uniform spatial distribution.

^c a fractal spatial density distribution and the fractal dimension is 2.5 in this research.

^d the dihedral angles equal to 60° and angle bisectors are parallel to σ_1 .

^e L_{max} is the maximum length of the fracture; a is the exponent of the power-law distribution.

where L is the system size, $p_c(L)$ is the percolation threshold in a finite-size system, p_c^∞ is the percolation threshold in a infinitely large system and $\Delta p_c(L)$ is the standard deviation of $p_c(L)$.

The results of I_{3D} and its standard deviations are shown in Fig. 7(a,d). For most scenarios, I_{3D} is not constant for fracture networks with different system sizes after accounting for the finite-size effect. Except for one region with $F_D = 2.1$ and exponent $a = 3$, referring to fracture systems composed of small fractures and having strong clustering effects, the variation of I_{3D} is relatively small in fracture networks of different sizes (from 10 to 40). However, from Fig. 7(d), standard

deviations of I_{3D} have not decreased with increasing system sizes for this region, indicating that no finite-size effects exist. Therefore, I_{3D} is not a valid percolation parameter in complex 3D fracture networks, consistent with the conclusion in Zhu et al. (2018). A larger system size and a wider range of exponents may yield better demonstrations as done in Zhu et al. (2018). However, the main focus of the work is to find percolation status in different dimensionalities instead of investigating the validity of I_{3D} as a percolation parameter. In addition, the cluster-check operation of 2D cross-section maps has to be implemented after each new 3D fracture is added to the system, which is highly time-consuming. Therefore, we limit the system size to be 40 as the maximum.

The fracture intensities P_{30} and P_{32} have similar trends as the 2D intensity parameters P_{20} and P_{21} . Both of them have their values decrease with increasing system sizes, indicating the scaling of the total number and total length of fractures is proportional to L^{D_s} , where D_s should be smaller than 3. This observation is consistent with observations in Bour and Davy (1997) and Bour and Davy (1998), where they considered the fracture network following a power-law length distribution and uniform position distribution in both 2D and 3D.

For P_{30} , P_{32} and I_{3D} , the exponent a positively and the system size L negatively correlate with them. The fractal dimension F_D has a weak correlation with intensity parameters but has a strong negative correlation with I_{3D} , meaning that clustering effects can increase intersections among fractures but have an insignificant impact on fracture intensities. To better explain this phenomenon, Fig. 8 shows examples of 10,000 spatial points following a uniform or fractal spatial density distribution with $F_D = 2.1$.

Compared with the uniformly distributed points, strong clustering effects exist in the fractal case, and many local clusters are formed in different parts of the domain. Those local clusters can significantly increase intersections of fractures and enhance local connectivity. However, the global connectivity seems not severely affected since 3D fractures can connect the other fractures in any direction. However, in 2D fracture networks, the linkage of fractures is constrained in the same plane, and clustering effects impact their fracture intensity and

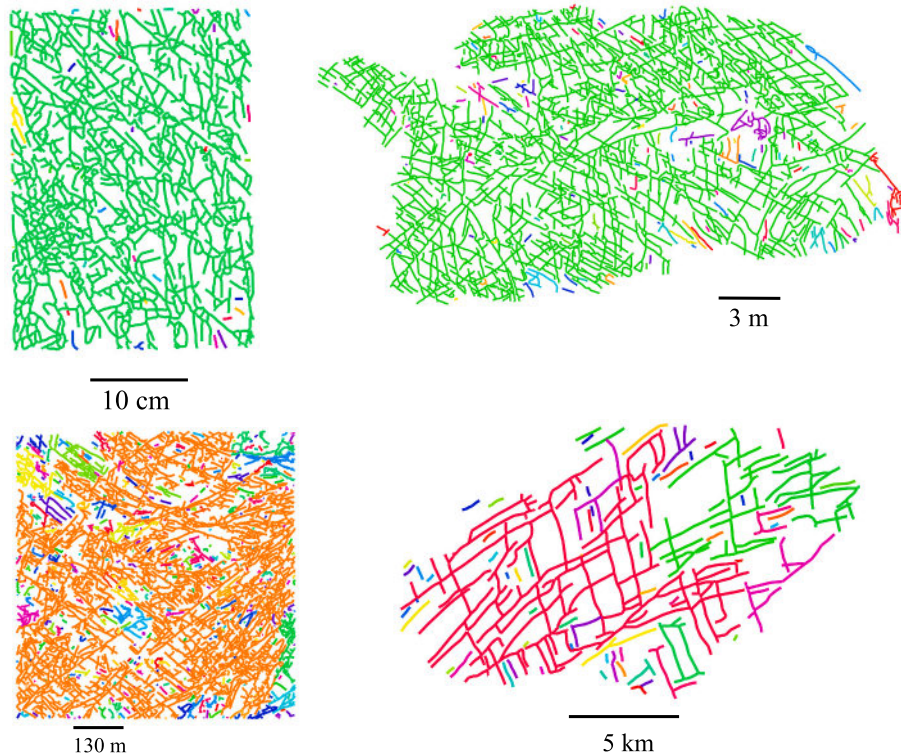


Fig. 17. Outcrop maps with different clusters checked (Odling, 1997; Holland et al., 2009b; Bertrand et al., 2015; Duffy et al., 2017). Each cluster is marked a different colour from its neighboring clusters.

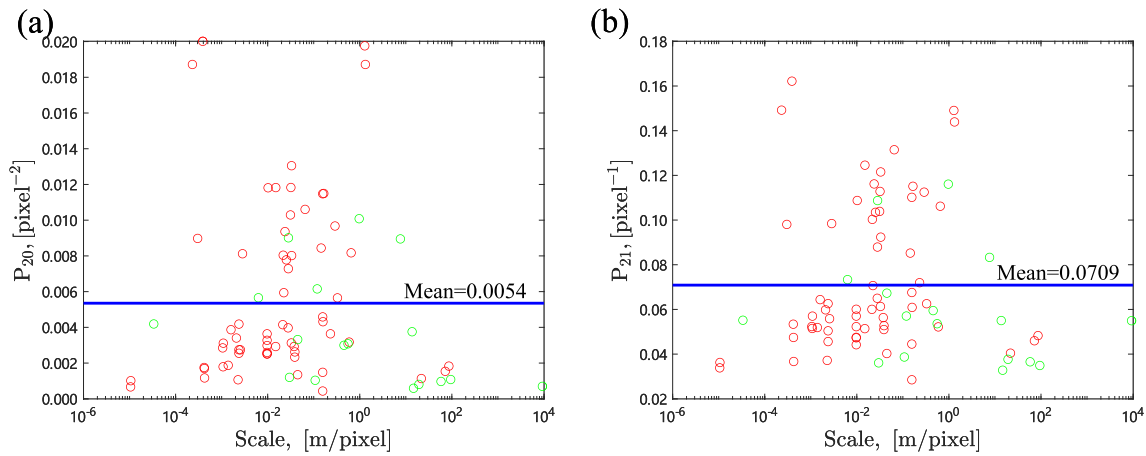


Fig. 18. Fracture intensities, P_{20} and P_{21} , of 80 published outcrop maps. Red data points refer to outcrops with a spanning cluster formed; Green data points refer to outcrops without a spanning cluster formed. (For interpretation of the references to colour in this figure legend, the reader is referred to the web version of this article.)

connectivity significantly. Those observations are consistent with the conclusion from Zhu et al. (2021c), where the impact of fracture geometries on the connectivity of 2D and 3D fracture networks are systematically investigated.

3.2. Results in phase two

For phase two, a spanning cluster is formed in a 2D cross-section map. This scenario is more likely to happen in reality because many outcrop maps show good connectivity. Fig. 1 shows two examples at the Achnashellach Culmination field area (Fig. 7B and D in Watkins et al. (2015)), where natural outcrop maps form spanning clusters, and the fracture intensity is much higher than the intensity at percolation. Figs. 9 and 10 have similar meanings with Figs. 6 and 7.

Fig. 9(a,d) shows the number of intersections per fracture (I_{2D}) in cross-section maps. I_{2D} has been corrected for finite-size effects since a spanning cluster is formed in the outcrop maps at phase two. However, I_{2D} does not keep constant, indicating I_{2D} is not a proper percolation parameter for complex fracture networks as observed in Zhu et al. (2018). The other two intensity parameters, P_{20} and P_{21} , have similar trends as results in phase one, but with much higher values (almost five times higher).

The fractal dimension here also has a negligible correlation with intensity parameters. However, this observation is inconsistent with conclusions in Zhu et al. (2021c), where clustering effects have a significant impact on the connectivity of 2D fracture networks. It is worthwhile to mention that the fractal spatial distribution in 3D fracture networks can bring clustering effects in 2D cross-section maps. However, it is different from clustering effects in 2D fracture networks, where their positions of fracture centers directly follow a fractal spatial density distribution. The clustering effects in the cross-section map highly depend on the position of the cross-sectional plane.

For comparison, we also generate 2D fracture networks with positions of fracture centers following a fractal spatial density distribution with the fractal dimension (F_D) varying between 1.2 and 2.0. Their lengths follow a power-law distribution with exponent (α) varying between 2.0 and 3.0, and orientations are uniformly distributed between 0 and π . The system size (L) varies between 10 and 40. Each scenario is stabilized by averaging over 50 realizations. The sensitivity of P_{20} , P_{21} and I_{2D} with respect to α , F_D and L are shown in Fig. 11. The results are systematically different from the correlations in Fig. 9(g-i). For I_{2D} , the exponent α and fractal dimension F_D have similar results as correlations in cross-section maps, but the system size has opposite results. For intensity parameters, P_{20} and P_{21} , the fractal dimension F_D has a positive correlation, indicating clustering effects actually can increase the

fracture intensity and can be significant to the connectivity of 2D fracture networks.

When a spanning cluster forms in the cross-section map, the corresponding 3D fracture network is over-percolative, with a much higher fracture intensity at percolation. In Fig. 10, intensity parameters, P_{30} and P_{32} , have much higher values compared with the results at percolation in Fig. 7, but keep similar trends. However, I_{3D} has an opposite trend compared with I_{3D} in phase one. When exponent α is small, I_{3D} has a higher value, indicating that large fractures can generate more intersections in dense fracture networks.

Furthermore, two phases can be linked with the ratios of fracture intensity parameters as introduced in Table 1. In particular, we show the number ratio (3D) and area ratio (3D) in Fig. 12. These ratios reflect the degree of over-percolation. A larger number ratio means the number of fractures in reality is much larger than the number of fractures required at percolation. There are several spikes in Fig. 12, especially in sub-figures (a) and (b). Those spikes usually happen with an intermediate exponent α , where a few large fractures can form the spanning cluster in the 3D fracture networks. However, many fractures are needed to form a spanning cluster in the cross-section map, making the ratio extremely large. A few anomalous values significantly increase the mean and standard deviation since only 50 realizations are implemented to stabilize the results. A larger number of realizations can make results smoother. However, it will not change the conclusion that the 3D fracture network has to be over-percolative when a spanning cluster is formed in its cross-section map.

Both number and area ratios have a weak correlation with all three parameters shown in Fig. 12, indicating that this phenomenon is common and independent of fracture geometries and system sizes. The area ratio has a relatively strong correlation with the power-law exponent, α , indicating systems dominated by small fractures may have a large area ratio.

Fig. 13 provides the histogram and cumulative distribution function of mean ratios. Detailed statistics of the number ratio and area ratio are summarized in Table 2. Both the number ratio and area ratio have a wide range of variations. The minimum value of the number ratio is 3.5, which can be regarded as a lower limit to predict the fracture intensity of 3D fracture networks based on their outcrop maps. If the outcrop map is well-connected and has a spanning cluster formed, the corresponding subsurface fracture network in 3D should form a spanning cluster and have an intensity at least 3.5 times larger than the intensity at percolation.

However, if the outcrop map is sparse and no spanning cluster is formed, can we infer any useful information on the connectivity of the corresponding 3D fracture networks? The number ratio or length ratio of

2D cross-section maps at two phases can provide a criterion to predict the formation of the spanning cluster in corresponding 3D fracture networks. The number ratio (2D) and length ratio (2D) are defined in Table 1. Take the number ratio equal to 0.3 as an example. If the fracture intensity is 0.3 times as large as the fracture intensity required to form the spanning cluster in an outcrop map, it is highly possible that a spanning cluster is formed in the corresponding 3D fracture network in the subsurface. Fig. 14 presents the mean values of the number ratio (2D) and length ratio (2D), their standard deviations, and sensitivity analysis. Fig. 14 (c,f) show that clustering effects and the system size have negligible impacts on the number ratio (2D) and length ratio (2D). The impact of the exponent is slightly higher and negative, indicating that larger fractures make the ratios smaller and easier to form a spanning cluster in 3D fracture networks. Fig. 15 provides the histogram and cumulative distribution function of the mean ratios, and both the number and length ratios have a similar distribution. Detailed statistics are summarized in Table 2. The maximum value of the number ratio (2D) is 0.43, and it can be regarded as a lower limit to predict the formation of a spanning cluster in 3D fracture networks. In practice, if outcrops are sparse, we can distribute new fractures following the same statistic distributions summarized from existing fractures, and terminate when a spanning cluster is formed. Then, check the number ratio between the original and percolative fracture networks. If the number ratio is larger than 0.43, a spanning cluster in the subsurface can be formed.

4. Discussion

The fracture networks concerned above have their fracture lengths, positions, and orientations follow a single stochastic distribution, respectively. A natural fracture network may be more regularized with different sets of fractures during their long geological history. Each fracture set has its own distributions. In this section, we constrain fracture networks with simple geomechanics principles and outcrop characteristics to make them more geologically meaningful. Similar approach is adopted in Zhu et al. (2019). To this effect, we have introduced four types of joints (Hodgson, 1961), sketched in Fig. 16a.

Type 1 joints are blue, and type 2 joints are green. These are tension joints that are approximately parallel and perpendicular to the hinge line. Type 3 conjugate shear joints (actually microfaults) are red. They have dihedral angles equal to 60° , and their angle bisectors parallel the maximum principal stress σ_1 . Type 4 shear joints (microfaults) are cyan. They have random strikes and dips because of the local anisotropy. The existence of random shear joints brings more complexity and uncertainties to the network. The system size is 100^3 of arbitrary units. The orientations of the maximum and minimum principal stress σ_1 , σ_3 are north-south and east-west, respectively. The distributions of fracture lengths, strike angles, dip angles, and the positions of fracture centers are listed in Table 3. A more detailed description of procedures to construct realistic 3D fracture networks can be found in Zhu et al. (2019). After generating the 3D fracture network, we take the cross-section map at the middle position, shown in Fig. 16(c). Compared with the natural outcrop in Fig. 16(b), the cross-section map is not identical, but they share many common characteristics, like preferential fracture orientations, and different fracture sets.

The total number of fractures in the 3D fracture networks is 49,979, and the entire area is 8,347,170. The largest cluster in the cross-section map is checked and marked in red. The cross-section map is over-percolative. Furthermore, the corresponding 3D fracture network is also over-percolative. After checking clusters, the number of fractures at percolation is 3222, and the total area is 543,271. Therefore, the number ratio between the total number of 3D fractures at the final stage and percolation is 15.5. The corresponding area ratio is 15.4. Therefore, our conclusion is valid in realistic fracture networks, where the 3D fracture network should be over-percolative if its outcrop map has a spanning cluster formed.

Renshaw et al. (2020) used ice as a model for rock and conducted

systematic experiments, where samples were subjected to uniaxial compressive loading. Their experiments observed that crack density remains nearly constant after the onset of percolation. They concluded that only limited fracture growth is possible after the onset of percolation. We collected 80 outcrop maps from different parts of the world and digitized the outcrop maps with an automatic fracture detection algorithm (Zhu et al., 2021a). 63 out of 80 maps have a spanning cluster formed and have their fracture intensities much larger than the intensity at percolation. Four outcrop maps at different scales (cm–km) are presented in Fig. 17 for demonstration. Each cluster is marked a different colour from its neighboring clusters. Fig. 18 shows the fracture intensity of all outcrop maps. Red circles refer to outcrop maps where a spanning cluster is formed. Green circles refer to outcrop maps where no spanning cluster is formed. The scales vary from millimeters to tens of kilometers. The fracture intensity parameters, P_{20} and P_{21} , are calculated for the entire map instead of local regions. Their values vary in a wide range and almost do not correlate with scales. The correlation coefficients between the scale and P_{20} , P_{21} are -0.1 and -0.06 , respectively. The independence of scales reveals the self-similar pattern of fracture networks in an aspect of the fracture intensity.

From observations of this research, the 3D fracture network has to be over-percolative if its cross-section map forms a spanning cluster. This conclusion is independent of fracture geometries and system sizes. If this conclusion is valid in reality, the corresponding subsurface fracture networks of those outcrop maps must be over-percolative and have a much higher intensity than the intensity at percolation. The conclusion from Renshaw et al. (2020)'s experiment is valid in their experimental environment, where the excess strain is accompanied by the opening of existing fractures rather than generating new fractures. For natural rocks existing for a long geological history, stress conditions changed, and different sets of fractures with various orientations (Watkins et al., 2015) were generated. Thus they can form complex and well-connected fracture networks.

It is also worth mentioning that the well-connected fracture networks cannot ensure good hydraulic conductivity of subsurface fracture networks because i, outcrops can only be regarded as relevant to the subsurface formation if the rock types and structural settings of the surface outcrops and subsurface formations are similar. However, weathering, stress-release during the upward movement, and complex surface topography can cause outcrops to differ from the subsurface systems significantly (Ukar et al., 2019); ii, compression and cementation can cause the closure and sealing of fractures over geologic time, which together significantly reduce the fracture permeability (Ito and Zoback, 2000). The hydraulic conductivity of subsurface fracture networks thus depends on many factors, such as sealing patterns, and current global and local stress states. More detailed investigations can be found in our previous research (Zhu et al., 2021a).

5. Conclusions

This research systematically investigates the percolation status of 3D fracture networks and their cross-section maps by assuming that the outcrop map is relevant to the subsurface structure and can be regarded as a cross-section map of the corresponding 3D fracture network. Several key conclusions are summarized:

- Clustering effects impact the local intersections significantly but have negligible impacts on fracture intensities of 3D fracture networks.
- The number of intersections per fracture, I_{2D} or I_{3D} , is not a proper percolation parameter for complex 2D and 3D fracture networks.
- Fracture intensities depend on the system size and usually decrease with increasing sizes.
- If the outcrop map has a spanning cluster formed, the corresponding natural fracture network in the subsurface should be over-

percolative and has its intensity at least 3.5 times larger than the intensity at percolation.

- If the 2D outcrop map is sparse and only local clusters are formed, but its intensity is larger than 0.43 times the intensity at percolation, the corresponding 3D fracture network can have a spanning cluster formed.

Data availability

All data are synthetically generated by our in-house built DFN modeling software, HatchFrac. The C++ code for generating 2D and 3D fracture networks is available online (<https://data.mendeley.com/datasets/zhs97tsdry/1>).

CRediT authorship contribution statement

Weiwei Zhu: Conceptualization, Methodology, Investigation, Writing – original draft. **Gang Lei:** Investigation, Writing – original draft, Resources. **Xupeng He:** Investigation, Data curation. **Yafan Yang:** Investigation, Visualization, Software. **Ryan Kurniawan Santoso:** Investigation, Visualization. **Moran Wang:** Conceptualization, Supervision, Writing – review & editing, Project administration, Funding acquisition.

Declaration of Competing Interest

The authors declare that they have no known competing financial interests or personal relationships that could have appeared to influence the work reported in this paper.

Acknowledgments

This project was supported by the National Key Research and Development Program of China (No. 2019YFA0708704). The authors would like to thank all editors and anonymous reviewers for their comments and suggestions.

References

- Akara, M.E.M., Reeves, D.M., Parashar, R., 2021. Impact of horizontal spatial clustering in two-dimensional fracture networks on solute transport. *J. Hydrol.* 603, 127055.
- Barton, C., Larsen, E., 1985. Fractal geometry of two-dimensional fracture networks at yucca mountain, southwestern nevada. In: *International Symposium on Fundamentals of Rock Joint*, pp. 77–84.
- Berkowitz, B., 2002. Characterizing flow and transport in fractured geological media: a review. *Adv. Water Resour.* 25, 861–884.
- Berkowitz, B., Bour, O., Davy, P., Odling, N., 2000. Scaling of fracture connectivity in geological formations. *Geophys. Res. Lett.* 27, 2061–2064.
- Bertrand, L., Géraud, Y., Le Garzic, E., Place, J., Diraison, M., Walter, B., Haffen, S., 2015. A multiscale analysis of a fracture pattern in granite: a case study of the tamariu granite, catalunya, Spain. *J. Struct. Geol.* 78, 52–66.
- Bonnet, E., Bour, O., Odling, N.E., Davy, P., Main, I., Cowie, P., Berkowitz, B., 2001. Scaling of fracture systems in geological media. *Rev. Geophys.* 39, 347–383.
- Bour, O., Davy, P., 1997. Connectivity of random fault networks following a power law fault length distribution. *Water Resour. Res.* 33, 1567–1583.
- Bour, O., Davy, P., 1998. On the connectivity of three-dimensional fault networks. *Water Resour. Res.* 34, 2611–2622.
- Dershowitz, W.S., Herda, H.H., et al., 1992. Interpretation of fracture spacing and intensity. In: *The 33th US Symposium on Rock Mechanics (USRMS)*. American Rock Mechanics Association.
- Dershowitz, W., Hermanson, J., Follin, S., Mauldon, M., et al., 2000. Fracture intensity measures in 1-D, 2-D, and 3-D at Åspö, Sweden. In: *4th North American Rock Mechanics Symposium*. American Rock Mechanics Association.
- Duffy, O.B., Nixon, C.W., Bell, R.E., Jackson, C.A.L., Gawthorpe, R.L., Sanderson, D.J., Whipp, P.S., 2017. The topology of evolving rift fault networks: single-phase vs multi-phase rifts. *J. Struct. Geol.* 96, 192–202.

- Ellefsen, K.J., Hsieh, P.A., Shapiro, A.M., 2002. Crosswell seismic investigation of hydraulically conductive, fractured bedrock near mirror lake, New Hampshire. *J. Appl. Geophys.* 50, 299–317.
- Hodgson, R.A., 1961. Classification of structures on joint surfaces. *Am. J. Sci.* 259, 493–502.
- Holland, M., Saxena, N., Urai, J., 2009a. Evolution of fractures in a highly dynamic thermal, hydraulic, and mechanical system - (ii) remote sensing fracture analysis, jabal shams, oman mountains. *GeoArabia* 14, 163–194.
- Holland, M., Saxena, N., Urai, J.L., 2009b. Evolution of fractures in a highly dynamic thermal, hydraulic, and mechanical system-(ii) remote sensing fracture analysis, jabal shams, oman mountains. *GeoArabia* 14, 163–194.
- Hoshen, J., Kopelman, R., 1976. Percolation and cluster distribution. I. Cluster multiple labeling technique and critical concentration algorithm. *Phys. Rev. B Condens. Matter* 14, 3438.
- Ito, T., Zoback, M.D., 2000. Fracture permeability and in situ stress to 7 km depth in the KTB scientific drillhole. *Geophys. Res. Lett.* 27, 1045–1048.
- Jing, L., Stephansson, O., 2007. The basics of fracture system characterization—field mapping and stochastic simulations. In: *Developments in Geotechnical Engineering*, vol. 85. Elsevier, pp. 147–177.
- Lei, Q., Latham, J.P., Tsang, C.F., 2017. The use of discrete fracture networks for modelling coupled geomechanical and hydrological behaviour of fractured rocks. *Comput. Geotech.* 85, 151–176.
- Makarov, P., 2007. Evolutionary nature of structure formation in lithospheric material: universal principle for fractality of solids. *Russ. Geol. Geophys.* 48, 558–574.
- Masahi, M., King, P.R., Nurafza, P.R., et al., 2007. Fast estimation of connectivity in fractured reservoirs using percolation theory. *SPE J.* 12, 167–178.
- Mourzenko, V., Thovert, J.F., Adler, P., 2005. Percolation of three-dimensional fracture networks with power-law size distribution. *Phys. Rev. E* 72, 036103.
- Newman, M.E., Ziff, R.M., 2001. Fast Monte Carlo algorithm for site or bond percolation. *Phys. Rev. E* 64, 016706.
- Odling, N.E., 1997. Scaling and connectivity of joint systems in sandstones from western Norway. *J. Struct. Geol.* 19, 1257–1271.
- Renshaw, C.E., Schulson, E.M., Iliescu, D., Murzda, A., 2020. Increased fractured rock permeability after percolation despite limited crack growth. *J. Geophys. Res.: Solid Earth* 125, e2019JB019240.
- Rijks, E., 1990. Attribute extraction: An important application in any detailed 3-d interpretation study. In: *1990 SEG Annual Meeting, OnePetro*.
- Robinson, P., 1983. Connectivity of fracture systems—a percolation theory approach. *J. Phys. A Math. Gen.* 16, 605.
- Stauffer, D., Aharony, A., 1994. *Introduction to Percolation Theory*. CRC Press.
- Ukar, E., Laubach, S.E., Hooker, J.N., 2019. Outcrops as guides to subsurface natural fractures: example from the Nikanassin Formation tight-gas sandstone, Grande Cache, Alberta foothills, Canada. *Mar. Pet. Geol.* 103, 255–275.
- Wang, X., Crosta, G.B., Clague, J.J., Stead, D., Sun, J., Qi, S., Liu, H., 2021. Fault Controls on Spatial Variation of Fracture Density and Rock Mass Strength within the Yarlung Tsangpo Fault Damage Zone (Southeastern Tibet). *Eng. Geol.* p. 106238.
- Watkins, H., Bond, C.E., Healy, D., Butler, R.W., 2015. Appraisal of fracture sampling methods and a new workflow to characterise heterogeneous fracture networks at outcrop. *J. Struct. Geol.* 72, 67–82.
- Whitaker, A.E., Engelder, T., 2005. Characterizing stress fields in the upper crust using joint orientation distributions. *J. Struct. Geol.* 27, 1778–1787.
- Williams, J.H., Johnson, C.D., 2004. Acoustic and optical borehole-wall imaging for fractured-rock aquifer studies. *J. Appl. Geophys.* 55, 151–159.
- Wilt, M., Alumbaugh, D., Morrison, H., Becker, A., Lee, K.H., Deszcz-Pan, M., 1995. Crosswell electromagnetic tomography: System design considerations and field results. *Geophysics* 60, 871–885.
- Xu, W., Zhang, Y., Li, X., Wang, X., Ma, F., Zhao, J., Zhang, Y., 2020. Extraction and statistics of discontinuity orientation and trace length from typical fractured rock mass: a case study of the xinchang underground research laboratory site, China. *Eng. Geol.* 269, 105553.
- Zhu, W., Khirevich, S., Patzek, T., 2018. Percolation properties of stochastic fracture networks in 2D and outcrop fracture maps. In: *80th EAGE Conference and Exhibition 2018*.
- Zhu, W., Yalcin, B., Khirevich, S., Patzek, T., 2019. Correlation analysis of fracture intensity descriptors with different dimensionality in a geomechanics-constrained 3d fracture network. In: *Petroleum Geostatistics 2019, European Association of Geoscientists & Engineers*, pp. 1–5.
- Zhu, W., He, X., Santoso, R.K., Lei, G., Patzek, T., Wang, M., 2021a. Enhancing fracture network characterization: a data-driven, outcrop-based analysis. *Earth and Space Science Open Archive* 35. <https://doi.org/10.1002/essoar.10508232.1>. URL:
- Zhu, W., Khirevich, S., Patzek, T.W., 2021b. Hatchfrac: a fast open-source dfn modeling software. *Earth and Space Science Open Archive* 44.
- Zhu, W., Khirevich, S., Patzek, T.W., 2021c. Impact of fracture geometry and topology on the connectivity and flow properties of stochastic fracture networks. *Water Resour. Res.* e2020WR028652.